Nanoparticles

DOI: 10.1002/anie.201207177

Ligand-Shell-Directed Assembly and Depolymerization of Patchy Nanoparticles**

*Offer Zeiri, Yifeng Wang, Alevtina Neyman, Francesco Stellacci, and Ira A. Weinstock**

Patchy nanoparticles (PNs) are particles coated with mixtures of ligand molecules that separate to form domains or "patches" of various geometries and dimensions.[1] One of the main attractive features of PNs is that they can engage in directional interactions, and as a consequence, self-assemble into complex yet predictable structures.[2] PNs are starting to be used in applications ranging from molecular recognition[3] to cell membrane penetration.[4] For many applications, monolayer-protected gold nanoparticles (Au NPs) are used as remarkably versatile precursors to a wide variety of patchy-particle building blocks.[2c,5] The Au NPs have a central core, the size and shape of which can be readily changed, and their protecting ligands can possess a wide range of physical and chemical properties. Moreover, advances in understanding[6] now make it possible to design mixed-monolayer shells with predictable patchy protecting-ligand domains on the Au-NP surface.[7]

Recently we began studying a new class of Au PNs: particles stabilized by mixtures of alkanethiolate and inorganic polyoxometalate (POM) cluster-anion protecting ligands,[8] such as α-$AlW_{11}O_{39}^{9-}$ (**1**, Figure 1).[9] The combination of small organic molecules bound to the NP surface through Au–S bonds with the much larger and negatively charged inorganic anions provides an extreme situation, which is different from anything studied before. Moreover, owing to their numerous tungsten ($Z = 74$) atoms, the POMs enable us to directly image PN ligand shells by cryogenic transmission electron microscopy (cryo-TEM).[10]

Our initial studies focused on the replacement of anionic POM ligands by thiol ligands possessing anionic carboxylate endgroups. On approximately spherical POM-protected Au NPs, we observed the formation of small islands of the thiolate ligands, and these islands grew as a function of thiol concentration.[11] We also recently observed that for tetrahedral and octahedral POM-protected Au NPs, the place exchange of POMs by the anionic thiol ligands begins at the edges of the polyhedral particles.[7b]

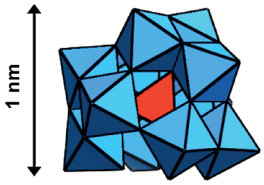

Figure 1. Structure of α-$AlW_{11}O_{39}^{9-}$ (**1**) in polyhedral notation. Color code: W^{VI}-centered polyhedra: blue, Al^{III}-centered tetrahedron: red. Oxygen atoms are located at the vertices of the polyhedra.

Herein we present a more complex situation, the exchange of POM anions by a cationic alkanethiol, HS-$(CH_2)_{11}N(CH_3)_3^+$ (HSR^+). Analogously to what has been found previously for systems consisting of only alkanethiolates,[6c,7a] we identify two distinct size regimes (Figure 2).

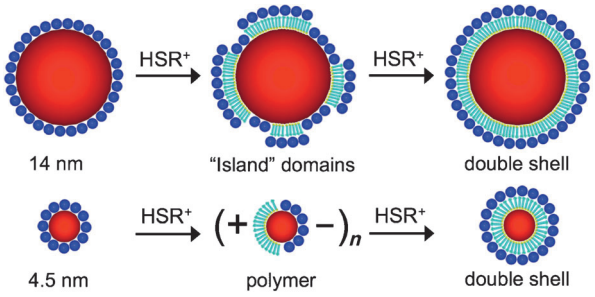

Figure 2. Reactions of gold nanoparticles (red spheres) that are protected with **1** (blue circles) with a cationic thiol containing a quaternary ammonium endgroup (cyan-colored rods with small yellow dots representing the thiol group).

For **1**-protected Au NPs with a diameter of 14 nm, partial exchange gives rise to the formation of numerous patches. For smaller, 4 nm Au NPs, partial ligand exchange leads to the formation of Janus nanoparticles. These Janus particles in turn form long linear aggregates. Notably, upon or close to complete exchange, particles of both sizes form three-component core–shell aggregates never observed before in PNs: namely, a corona of POM cluster anions forms around a spherical shell of cationic thiolate ligands bound directly to the gold surface (far right in Figure 2). We herein provide

[*] O. Zeiri, Dr. Y. Wang, A. Neyman, Prof. I. A. Weinstock
Department of Chemistry and the Ilse Katz Institute for Nanoscale Sciences and Technology, Ben Gurion University of the Negev
Beer Sheva, 84105 (Israel)
E-mail: iraw@bgu.ac.il
Homepage: http://www.bgu.ac.il/~iraw/Home.html
Prof. F. Stellacci
Institute of Materials
École Polytechnique Fédérale de Lausanne (EPFL)
Lausanne (Switzerland)
and
Department of Materials Science and Engineering
Massachusetts Institute of Technology
Cambridge, MA 02139 (USA)

[**] I.A.W. and F.S. thank the United States-Israel Binational Science Foundation (2008277), and I.A.W. thanks the Israel Science Foundation (248/09), for support. We thank Prof. Jacob Klein for input regarding counterion release.

Supporting information for this article is available on the WWW under http://dx.doi.org/10.1002/anie.201207177.

a full description of these phenomena and propose a reasonable framework from which all of them can be understood.

To obtain quantitative reference points for controlled additions of HSR^+, a published spectroscopic method[11] involving titration with mercaptoundecanoate (HSR^-) was used to fully displace **1** from the Au-NP surfaces. In these UV/Vis titrations, complete displacements of **1** are indicated by well-defined titration "endpoints" (see Figure S1 in the Supporting Information), which provide quantitative reference values for additions of HSR^+. (As shown below, HSR^+ is not suitable for direct use in these titrations.)

After HSR^+ was added to **1**-protected Au NPs with a diameter of (13.8 ± 0.1) nm (Figure 3a) to give a final concentration equal to 100% of the HSR^- endpoint, cryo-

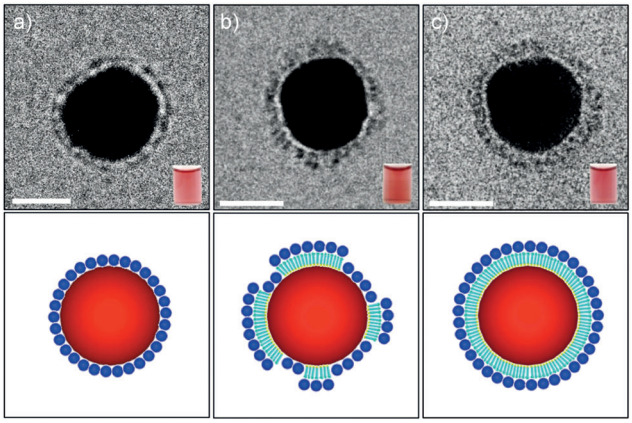

Figure 3. Reaction of a **1**-protected 14 nm Au NP with HSR^+. Shown are cryo-TEM images of 14 nm Au NPs: a) protected by a monolayer of **1**, b) after adding HSR^+ to give a concentration equal to 50% of the HSR^- endpoint value, and c) after adding HSR^+ to a concentration equal to 100% of the HSR^- endpoint value, thereby resulting in a core/double-shell structure. Two-dimensional illustrations are provided below each cryo-TEM image. Scale bar = 10 nm. Insets show pictures of the corresponding solutions.

TEM images revealed a spherical shell of intensity surrounding the Au cores (Figure 3c and Figure S2 in the Supporting Information). The thiolate ligands are not observed by cryo-TEM.[7b,11] Rather, POMs provide the intensity associated with the spherical shell around the Au core. The distance from the Au core to the outer surface of the **1**-monolayer shell in Figure 3a is (1.5 ± 0.1) nm.[10a,12] After addition of HSR^+, the shell thickness (Figure 3c) had increased to (2.6 ± 0.4) nm (based on >100 measurements), the sum of the length of HSR^+ (ca. 1.5 nm) and the crystallographic diameter of the POM anion (1.2 nm).[12] Furthermore, the hydrodynamic radius of the particles (from dynamic light scattering, DLS) increased by (1.8 ± 0.3) nm.

Additional information about the mixed-ligand shell was provided by UV/Vis spectroscopy. When HSR^+ was incrementally added to **1**-protected 14 nm gold nanoparticles, surprisingly small spectral changes were observed. No changes are detected at 750 nm (Figure 4, blue circles), thus ruling out particle aggregation. The surface plasmon resonance (SPR) absorbance maximum remained at 526 nm,

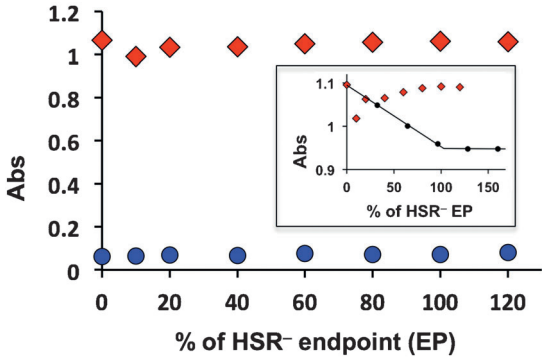

Figure 4. UV/Vis absorbance changes upon incremental additions of HSR^+ to **1**-protected 14 nm Au NPs. Concentrations of HSR^+ are plotted relative to the HSR^- endpoint (EP). Absorbance at 526 nm is shown by red diamonds, and at 750 nm by blue circles. Uncertainties (from repeated reactions) are 0.017 and 0.006 arbitrary units, respectively. Inset: Comparison of the absorbance at 526 nm during additions of HSR^+ (red diamonds), with the linear decrease in absorbance during the displacement of **1** by HSR^-, leading to the titration endpoint (black circles and line).

slightly decreased in intensity at first, but returned to 99% of its initial value as $[HSR^+]$ reached 100% of the HSR^- endpoint concentration (i.e., 100% EP; Figure 4, red diamonds). By contrast, displacement of **1** from the ligand shell by HSR^- (in solutions with pH ca. 7) causes a linear decrease in SPR absorbance, thereby leading to a titration endpoint (noted above) as the POMs are not only removed from the Au surface, but are subsequently repulsed by the organic ligands' anionic (carboxylate) endgroups (Figure 4, inset).

The very small (1%) decrease in absorbance at 526 nm after HSR^+ was added to $[HSR^+] = 100\%$ EP confirms that nearly all of the 330[10a] molecules of **1** initially in the POM-monolayer shell remain relatively close to the gold surface. Importantly, the SPR absorbance remains largely unchanged, because it is still determined by the refractive index of an encapsulating inorganic-ligand shell.[13]

These data indicate a clean "insertion" of the cationic thiolate ligands, thus giving the double-shell structure illustrated below Figure 3c; this structure is comprised of a gold core with an alkanethiolate protecting shell, surrounded by a spherical shell of POM anions electrostatically stabilized[10b] by interaction with the cationic endgroups of the self-assembled monolayer (SAM) of -SR^+ ligands.

The above methods were used to assess the intermediate structures formed during incremental additions of HSR^+. Initially, ($[HSR^+] = 10\%$ EP, possibly corresponding to nucleation of HSR^+ on the Au surface), the absorbance at 526 nm (red diamonds in Figure 4 and its inset) indicated a decrease in the number of POMs in the mixed-ligand shell. When more HSR^+ was added ($[HSR^+] = 10$–100% EP), however, the absorbance at 526 nm returned to near its original value, thus suggesting the presence of more molecules of **1** near the Au particle (either on the Au surface, or forming ion pairs with larger patches of Au-bound -SR^+ ligands). Cryo-TEM images of intermediate ligand-shell structures at $[HSR^+] = 50\%$ EP (Figure 3b, and see also Figure S3 in the Supporting Information) revealed patches of

1 directly bound to the gold surface, along with regions in which the POM anions are farther from the surface and, we believe, associated with cationic endgroups of the -SR^+ ligands.

Next, HSR^+ was added to **1**-protected Au NPs with smaller, (3.8 ± 0.6) nm cores (Figure 5a). At [HSR^+] = 100% EP, ligand insertion gives double-shell structures (Figure 5c; see also Figure S4 in the Supporting Information) analogous to those on 14 nm particles. The thickness of the shell around the Au core increased to (2.3 ± 0.4) nm (based on > 100 measurements), relatively small changes were observed in UV/Vis spectra (Figure S5), and particle radii (by DLS) increased by (1.2 ± 0.3) nm.

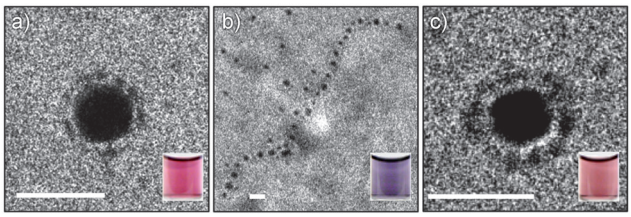

Figure 5. Reaction of HSR^+ with **1**-protected small Au NPs. a) Cryo-TEM image of a **1**-protected Au NP. b) Reaction with HSR^+ (40% EP) gives a purple solution (inset) owing to the formation of Au-NP polymers. c) Further addition of HSR^+ results in a disappearance of the purple color (depolymerization) and formation of a double-shell structure. (For cryo-TEM imaging, particles slightly larger than the average size of 4 nm were optimal: the core sizes of the particles in panels (a) and (c) are 5.5 nm and 5.0 nm, respectively.) Scale bar = 10 nm.

Remarkably, however, partial displacement of the POMs from the gold surface by HSR^+ ([HSR^+] = 40% EP) gave rise to purple solutions, and cryo-TEM images reveal linear polymers (Figure 5b and inset; see Figure S6 in the Supporting Information for UV/Vis spectra). Other cryo-TEM images revealed chains reaching lengths of up to several microns, and comprised of up to approximately 2000 particles (Figure S7 in the Supporting Information). In most of these large structures, branch points occur at approximately 5–15% of the monomeric units. Close examination of the images suggests the branching is due to the slightly polydisperse size distribution of the Au NPs with smaller (≤ 2 nm) particles acting as branching points. The Au-NP polymer solutions are remarkably stable, with no precipitate observed after months at ambient temperature. It seems that **1** plays an important role for stabilization as well. Namely, in the absence of **1**, the NPs of the same size with mixed ligand shells of 40 or 50% each of -SR^+ and -SR^- rapidly precipitate, thereby leaving clear, colorless solutions.

To form linear polymers (Figure 5b), the monomeric gold-core building blocks must contain functional regions on opposite sides of the approximately spherical particles. This structural motif, which is fundamental to polymer science, is the basis for covalently linked oligomeric chains of Au-NP oligomers,[14] and for the chains that arise from hydrophobic interactions between alkanethiolate capping ligands at opposite ends of 200 nm gold nanorods.[15] In the present case, the observation of highly linear polymers with abundant bifunctional Au-NP units suggests the formation and electrostatic assembly of dipolar Janus-like nanoparticles with phase-separated -SR^+ (positive) and inorganic cluster-anion (negative) ligand domains.

Experimental[7a] and computational[6c] data show that for sufficiently small Au cores, mixed-ligand shells phase separate to give Janus particles. Evidence for phase separated alkanthiolate and POM domains on the smaller (4 nm) Au cores was obtained by reacting **1**-protected particles with HSR^-. Owing to the negative charge of the thiolate, Au cores with mixed -SR^-/POM ligand shells remain as isolated particles, the mixed-ligand protecting-shell structures of which are more amenable to detailed analysis by cryo-TEM.[16] HSR^- ([HSR^-] = 20% EP)[17] was added to 4 nm Au NPs protected by mono-defect Wells–Dawson anions, α-$P_2W_{17}O_{61}^{10-}$ (**2**, K^+ salt). These cluster anions, each containing 17 W atoms, are more electron-dense than **1**, and more readily imaged (Figure 6; see also Figure S8 in the Supporting Information).

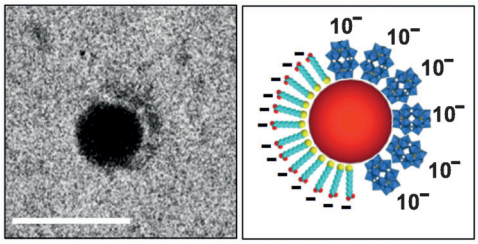

Figure 6. Phase-separated (Janus-like) mixed-ligand shells on small Au NPs. a) Cryo-TEM image of a (4 ± 1) nm Au core, protected by α-$P_2W_{17}O_{62}^{10-}$ (**2**), and then reacted with HSR^- (20% EP). b) Two-dimensional illustration of the image in (a). Scale bar = 10 nm.

Consistent with recent findings,[6c,7a] the -SR^- ligands appear to form single hydrophobic domains on the **2**-protected 4 nm Au cores, thereby resulting in Janus-like patchy nanoparticles with organic and inorganic (-SR^- and POM) regions. Hydrophobic domains, based on close interactions between the hydrocarbon chains of -$S(CH_2)_{11}N(CH_3)_3^+$ (-SR^+) should also be energetically favored when HSR^+ is added to **1**-protected 4 nm Au NPs. The length of -SR^+ is similar to the diameter of **1**, such that intimate mixing of the two ligands is not expected to enhance the conformational degrees of freedom (i.e., entropy) of the organic ligands. Rather, the positively charged endgroups would interact with neighboring cluster anions, thereby significantly decreasing conformational degrees of freedom of the hydrocarbon chains. Moreover, the inorganic monolayer is electrostatically stabilized by structurally integrated counter cations (Na^+ and K^+), that nearly balance the negative charges of the closely spaced cluster anions **1**.[10a,b] Hence, despite their cationic endgroups, the "intrusion" of -SR^+ ligands, with their hydrophobic 11-carbon-atom chains, into regions covered by monolayers of **1**, should be much less energetically favorable than separated domains, analogous to those in Figure 6.

Evidence that the ligand-shell structures of the self-assembled Au PNs are thermodynamically stable phase-

separated domains of -SR^+ and **1** was provided by examining a purple solution of the polymer (identical to that in Figure 5b) after storage for 18 months at ambient temperature (ca. 15 to 40 °C), unprotected from exposure to light. No precipitate was observed, and no changes were detected by UV/Vis spectroscopy (Figure S9 in the Supporting Information). The phase-separated domains of -SR^+ and **1** give rise to oppositely charged hemispherical regions. Electrostatic interactions between the positively and negatively charged domains of these "bifunctional" particles then direct the assembly of (predominantly) linear polymers (Figure 5b).

Additional support for this assembly mechanism is provided by comparison with the behavior of the larger, 14 nm diameter, Au PNs, of which the mixed-ligand shells consisting of **1** and -SR^+ ([HSR^+] = 50% EP) contain multiple patches of organic and inorganic domains (Figure 3b). In that case, no aggregation is detected by UV/Vis spectroscopy (blue circles in Figure 4). Owing to the presence of multiple patches, the particle's "faces" are heterogeneously charged. Hence, when the particles approach one another, the net electrostatic attraction is substantially smaller than that arising from the phase-separated ligand shells on the dipolar (Janus-like) 4 nm Au PNs.

Further consideration raises a fundamental question regarding the energetics of the electrostatic assembly process. Reaction of HSR^+ ([HSR^+] = 50% EP) with the inorganic-monolayer shell of a **1**-protected 4 nm Au NP is expected to give the intermediate structure at the upper right in Figure 7, in which POMs are ion-paired with the newly inserted -SR^+ ligands.

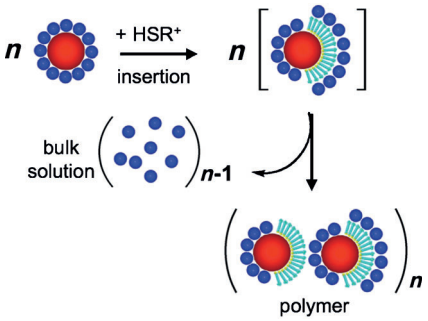

Figure 7. Entropically driven assembly involving the release of POM anions (blue spheres) to bulk solution.

Subsequent assembly gives the polymeric structure at the lower right in Figure 7. At the same time, the concentration of K_9**1** present in bulk solution is 2 mM, which is orders of magnitude larger than the approximately 10^{-8} M concentration of Au PNs. This high concentration of K_9**1** might be expected to prevent polymerization by favoring the intermediate structure at the upper right, in which molecules of **1** remain ion-paired to the positively charged -SR^+-ligand domain. (Associations of this type are precisely what we believe are responsible for the double-shell structures in Figure 3c and Figure 5c.)

However, theoretical analyses of the energetics of oppositely charged spherical particles show that aggregation is driven by the favorable entropy changes that accompany "counterion release".[18] As attraction between oppositely charged regions brings the particles closer to one another, counterions (in this case, molecules of **1**) are released into bulk solution (Figure 7, right and center), thus giving the polymeric assembly at the lower right. In related aggregations of oppositely charged particles, calculated changes in electrostatic energy range from slightly unfavorable to mildly favorable, as functions of particle radius, a, and the inverse Debye length, κ.[19] Changes in entropy, however, are consistently favorable. For the present case of (related) 4 nm particles (a = ca. 1.5 nm, and $\kappa = 1\ nm^{-1}$), large entropy changes are expected[19] to accompany the release of counterions[20] during polymerization.[21]

After polymerization, the addition of more HSR^+, to a final concentration equal to 100% EP (with mild warming), results in nearly quantitative depolymerization to give the double-shell structures shown in Figure 5c. This is a remarkable result, since, apart from a few notable exceptions,[22a] gold-nanoparticle assembly processes are irreversible.[22b] In the present case, however, depolymerization results from a simple transformation from dipolar to spherically symmetrical ligand shells.

More generally, the above findings show how the formation and behavior of patchy nanoparticles in solution—including the electrostatic self-assembly of micron-sized polymers and their subsequent depolymerization—can be controlled by choice of gold-core size combined with rational in situ modifications of mixed ligand-shell composition and structure.[2c]

Received: September 4, 2012
Published online: November 23, 2012

Keywords: gold · janus particles · nanoparticles · polyoxometalates · self-assembly

[1] a) I. C. Pons-Siepermann, S. C. Glotzer, *ACS Nano* **2012**, *6*, 3919–3924; b) I. C. Pons-Siepermann, S. C. Glotzer, *Soft Matter* **2012**, *8*, 6226–6231.
[2] a) E. Jankowski, S. C. Glotzer, *Soft Matter* **2012**, *8*, 2852–2859; b) K. Liu, Z. Nie, N. Zhao, W. Li, M. Rubinstein, E. Kumacheva, *Science* **2010**, *329*, 197–200; c) M. Grzelczak, J. Vermant, E. M. Furst, L. M. Liz-Marzán, *ACS Nano* **2010**, *4*, 3591–3605; d) F. Wurm, A. F. M. Kilbinger, *Angew. Chem.* **2009**, *121*, 8564–8574; *Angew. Chem. Int. Ed.* **2009**, *48*, 8412–8421.
[3] X. Liu, Y. Hu, F. Stellacci, *Small* **2011**, *7*, 1961–1966.
[4] A. Verma, O. Uzun, Y. Hu, Y. Hu, H.-S. Han, N. Watson, S. Chen, D. J. Irvine, F. Stellacci, *Nat. Mater.* **2008**, *7*, 588–595.
[5] a) S. Pradhan, L.-P. Xu, S. Chen, *Adv. Funct. Mater.* **2007**, *17*, 2385–2392; b) F. Stellacci, *Nat. Mater.* **2005**, *4*, 113–114.
[6] a) A. Santos, J. A. Millan, S. C. Glotzer, *Nanoscale* **2012**, *4*, 2640–2650; b) P. Guo, R. Sknepnek, M. O. de La Cruz, *J. Phys. Chem. C* **2011**, *115*, 6484–6490; c) C. Singh, P. K. Ghorai, M. A. Horsch, A. M. Jackson, R. G. Larson, F. Stellacci, S. C. Glotzer, *Phys. Rev. Lett.* **2007**, *99*, 226106.
[7] a) H. Kim, R. P. Carney, J. Reguera, Q. K. Ong, X. Liu, F. Stellacci, *Adv. Mater.* **2012**, *24*, 3857–3863; b) Y. Wang, O. Zeiri, L. Meshi, F. Stellacci, I. A. Weinstock, *Chem. Commun.* **2012**, *48*, 9765–9767; c) J. Du, R. K. O'Reilly, *Chem. Soc. Rev.* **2011**, *40*,

2402 – 2416; d) A. M. Jackson, J. W. Myerson, F. Stellacci, *Nat. Mater.* **2004**, *3*, 330 – 336.
[8] Y. Wang, I. A. Weinstock, *Chem. Soc. Rev.* **2012**, *41*, 7479 – 7496.
[9] I. A. Weinstock, J. J. Cowan, E. M. G. Barbuzzi, H. Zeng, C. L. Hill, *J. Am. Chem. Soc.* **1999**, *121*, 4608 – 4617.
[10] a) Y. Wang, A. Neyman, E. Arkhangelsky, V. Gitis, L. Meshi, I. A. Weinstock, *J. Am. Chem. Soc.* **2009**, *131*, 17412 – 17422; b) Y. Wang, O. Zeiri, S. Sharet, I. A. Weinstock, *Inorg. Chem.* **2012**, *51*, 7436 – 7438.
[11] Y. Wang, O. Zeiri, A. Neyman, F. Stellacci, I. A. Weinstock, *ACS Nano* **2012**, *6*, 629 – 640.
[12] S. Sharet, E. Sandars, Y. Wang, O. Zeiri, A. Neyman, L. Meshi, I. A. Weinstock, *Dalton Trans.* **2012**, *41*, 9849 – 9851.
[13] This result is consistent with the quite large sensitivity of the SPR to the index of refraction of the environment around the Au NP, combined with a long decay length of ca. 200 – 300 nm. See: A. J. Haes, S. Zou, G. C. Schatz, R. P. Van Duyne, *J. Phys. Chem. B* **2004**, *108*, 109 – 116.
[14] G. A. DeVries, M. Brunnbauer, Y. Hu, A. M. Jackson, B. Long, B. T. Neltner, O. Uzun, B. H. Wunsch, F. Stellacci, *Science* **2007**, *315*, 358 – 361.
[15] Z. Nie, D. Fava, M. Rubinstein, E. Kumacheva, *J. Am. Chem. Soc.* **2008**, *130*, 3683 – 3689.
[16] Efforts to obtain higher-magnification images of linkages between polymerized particles (such as those in Figure 5b) were frustrated by the small size and unique structures of the interparticle regions.
[17] At $[HSR^-] > 20\%$ EP, random orientations of the particles make it more difficult to find PNs optimallly aligned relative to the electron beam.
[18] A. A. Meier-Koll, C. C. Fleck, H. H. von Grünberg, *J. Phys. Condens. Matter* **2004**, *16*, 6041 – 6052.
[19] S. A. Palkar, A. M. Lenhoff, *J. Colloid Interface Sci.* **1994**, *165*, 177 – 194.
[20] POM-monolayer countercations are also "released" during polymerization, thus adding to the favorable entropy of polymerization.
[21] This requires that the net charges of the organic and inorganic regions are similar or differ by perhaps a factor of two. This is reasonable, because the charge of each molecule of **1** in the inorganic monolayer is nearly equalized by structurally integrated countercations.
[22] a) R. Klajn, P. J. Wesson, K. J. M. Bishop, B. A. Grzybowski, *Angew. Chem.* **2009**, *121*, 7169 – 7173; *Angew. Chem. Int. Ed.* **2009**, *48*, 7035 – 7039; b) S. Srivastava, N. A. Kotov, *Soft Matter* **2009**, *5*, 1146 – 1156.

